Atomistic Models of Amorphous Polybutadienes. 3. Static Free Volume

Sanjay Misra and Wayne L. Mattice*

Institute of Polymer Science, The University of Akron, Akron, Ohio 44325-3909

*Received April 1, 1993; Revised Manuscript Received September 29, 1993**

ABSTRACT: Atomistic models of polybutadiene have been generated using molecular mechanics and molecular dynamics at a bulk density of 0.89 g cm^{-3}. Four microstructures formed by *cis*-1,4-polybutadiene, *trans*-1,4-polybutadiene, 1,2-polybutadiene, and a random copolymer of the three (55% trans, 35% cis, and 10% vinyl) are analyzed for static free volume. The free volume is determined by hard spherical probes that see the atoms as hard spheres of radii which equal 89% of their van der Waals radii. The total free volume, the free volume distribution, and the shape of the voids are analyzed for all four microstructures. The accessible free volume as a function of the probe size is found to be characteristic of voids in disordered packings of hard spheres. The free volume distributions have some common features across the microstructures. In particular, the free volume distributions as probed by a 1-Å radius probe show void size concentrations around ~7.5 and 15 Å^3 (with the exception of *trans*-polybutadiene, which does not display the latter). The shape factors for all four structures decay to the same asymptotic value of 0.67 ± 0.1 over the size range of 0–5 Å^3. There is a marked difference in the asphericity and the acylindricity of voids in the four microstructures. Analysis of randomly generated shapes suggests that the voids in the polymer microstructures are mostly elongated in comparison with randomly "grown" cavities, probably due to the connectivity of the polymer chains.

1. Introduction

Atomistic modeling of amorphous polymeric systems is a powerful tool for studying microscopic properties of polymers as well as for predicting the properties of the bulk material. We have recently reported the results of atomistic modeling of amorphous polybutadiene, a commercially important polymer.[1,2] In those studies the focus was upon the conformational aspects of the polymer chains as well as upon intermolecular packing in the bulk. In this study we focus upon the static free volume in amorphous polybutadiene.

Free volume and its distribution have an important bearing upon the properties of amorphous polymers. The total amount of free volume, its size distribution, and its dynamics dominate phenomena involving the motion of polymer chains (viscosity and diffusion), at least in the vicinity of the glass transition temperature ($T_g < T < T_g + 100$ K). The viscosity behavior of polymer melts plays a central role in polymer processing. Diffusion of penetrants inside polymer matrices is of special importance in gas diffusion through packaging films and transport of plasticizers and lubricants or biological molecules through polymers.

Interest in the effects of free volume upon chain mobility has led to numerous experimental as well as theoretical works over the past 35 years. Some of the recent experimental studies have focused upon free volume dynamics,[3] aging and associated free volume changes,[4,5] chain dynamics and its relation to excess free volume,[6] free volume distribution and its dynamics,[7-9] and viscosity behavior of melts.[10] On the theoretical side, from the analysis of Cohen and Turnbull[11,12] on molecular transport in liquids, it is known that the probability of finding a void exceeding a certain critical volume, $P(v^*)$, determines the viscosity or diffusivity in a polymer melt. This probability is given by

$$P(v^*) = \exp\left(\frac{\gamma v^*}{v_f}\right) \quad (1)$$

Here γ is a numerical prefactor, v^* is a critical void volume which depends upon the size of the diffusing or jumping unit, and v_f is the average free volume per diffusing or jumping unit. The temperature effect in turn is manifested through the change in the free volume v_f with changing temperature.

Central to the predictions of the free volume based theories is the estimation of the free volume itself. Theoretical prediction of free volume is usually indirect and involves adjustable parameters. Free volume estimation has benefited greatly from the statistical mechanical theory of Simha and Somcynsky[13,14] for the bulk polymer state. This theory predicts the free volume of an amorphous melt through free energy minimization of the melt. The Simha–Somcynsky theory has been successful in the prediction and correlation of phenomena involving free volume and its dynamics. However, it is only recently, with the advent of atomistic models, that the free volume in amorphous polymers is being addressed as a nonadjustable parameter. Indeed, Shah et al.[15] generated atomistic models for polypropylene and poly(vinyl chloride) based upon Theodorou and Suter's method.[16] Using a Monte Carlo technique, they then determined the total static free volume as probed by hard spheres of various sizes. Arizzi et al.[17] have looked at free volume in atomistic polymer microstructures using Delaunay tessellation and analyzed the free volume distributions and the radii of gyration of the voids. In their molecular dynamics simulations, Rigby and Roe have analyzed free volume in polymeric liquids and glasses using both Voronoi tessellation and the hard probe method.[18] They look at the free volume distribution as well as the shape factor (dimensionless surface to volume ratio) of the voids. While the static amorphous cell models on the lines of Theodorou and Suter's work do not explicitly admit temperature as a variable, temperature enters indirectly through the

* Abstract published in *Advance ACS Abstracts*, November 15, 1993.

0024-9297/93/2226-7274$04.00/0

specification of the bulk density. Thus simulations performed at different bulk densities would essentially mimic changes in free volume with temperature.

The aim of the present work is to evaluate the free volume in amorphous polybutadiene as probed by hard spheres from the following perspectives. We analyze (i) the total free volume accessible to hard spheres, (ii) the void size distributions and, (iii) the shape of these voids. A comparison of the packing of hard spheres and polymer chains yields interesting qualitative insight into available free volume to hard probes. The shape analysis is twofold. The "roughness" of the surface of these voids is measured in the form of a shape factor which is a measure of the surface area to volume ratio of the voids. The symmetry of the voids is measured through their asphericity and acylindricity. We also generate random shapes, as discussed later, and compare their symmetry and shape factor to those obtained by voids in polymer microstructures. This provides a backdrop against which void shapes can be interpreted.

In section 2 we discuss briefly the atomistic model employed as well as the computational aspects involving the evaluation of the free volume. In section 3 the results of the computations are presented and discussed.

2. Atomistic Model and Free Volume

The atomistic model used to study amorphous polybutadiene has been discussed in detail elsewhere.[1,2] Here we shall mention the basics of the analyzed systems very briefly. Amorphous cells for *cis*-1,4-polybutadiene (*cis*-PBD), *trans*-1,4-polybutadiene (*trans*-PBD), 1,2-polybutadiene (*vinyl*-PBD), and a random copolymer of cis (35%), trans (55%), and vinyl (10%) units (*mixed*-PBD) were generated. The last corresponds to the composition of the typical commercially available polybutadiene. In all these cases chains comprising 99 monomers were placed in cubical cells which had a density of 0.89 g cm^{-3}—the cell edges were thus 21.514 Å. Periodic boundary conditions were employed in all three directions for generating the amorphous structures. The initial conformations were generated by a random assignment of the dihedral angles with the atoms assigned 30% of their van der Waals radii. These high-energy conformations were then subjected to conjugate gradient minimization followed by "shaking" and then another cycle of minimization (see refs 1 and 2 for details). The amorphous cell generation and the minimization were accomplished using the POLYGRAF 2.2 molecular modeling software provided by Molecular Simulations Inc.[19] Five cells for each PBD were thus equilibrated. These cells were assumed to have reached an energy minimum due to the similar final energies of the five cells, the agreement between the experiemntal and computed Hildebrand solubility parameters (with the exception of *vinyl*-PBD, for which no estimate is available), and a comparison with the RIS theory for the distribution of the rotational isomeric states.[1,2]

These cells were then subjected to free volume analysis where the free volume was determined by a hard spherical probe. The free volume calculations performed below correspond to a temperature of 300 K since the assigned bulk density of 0.89 g cm^{-3} is obtained at that temperature. The temperature dependence of the free volume is thus implicit in the assigned bulk density. A uniform grid was superposed upon the amorphous cells, the gridlines spaced by 0.25 Å (we thus divided the amorphous cell into "subcells" of size 0.25 Å). The carbon and hydrogen atoms were assumed to be hard spheres with radii which equaled 89% of their full van der Waals (vdW) radii. (The interatomic vdW interaction energy equals zero at this distance. Closer approach leads to an unfavorable positive interaction energy, and thus this distance is taken as the hard sphere radius of the atoms.) The probe was then allowed to "scan" the grid. In this procedure each atom was assigned an *effective* radius equaling the sum of its hard core radius and the probe radius. Subcells whose centers lay within the effective radius of any atom were assumed to be occupied. The unoccupied cells were counted as holes contributing to the free volume. This procedure is depicted in Figure 1. The whole grid, in this procedure, was divided into unoccupied and occupied subcells. To further analyze the distribution of the void sizes, the unoccupied subcells were scanned for connectivity. In case there were two or more adjacent free volume subcells that share a common face, they were assigned to the same void. This procedure leads directly to the size distribution of the voids. In all cases (*cis*-, *trans*-, *vinyl*-, and *mixed*-PBDs), the averages were performed over all five amorphous cells. We thus had a total of 49 789 $Å^3$ of volume of each bulk polymer to probe for free volume. Subsequent to the connectivity analysis, the volumes of the voids as well as the surface area enclosing them (exposed faces of the subcells) were computed. The radius of gyration tensors for these voids were also computed and transformed to their principal coordinate axes. From the radii of gyration were inferred the asphericity and the acylindricity of the voids. We also generated random shapes as a backdrop against which the void shapes could be inferred. These were obtained by growing random aggregates of cubes. In this process a growing aggregate was scanned for free faces and then the next cube was added at a randomly selected face. Cubes were added to the aggregate until the desired aggregate size was reached.

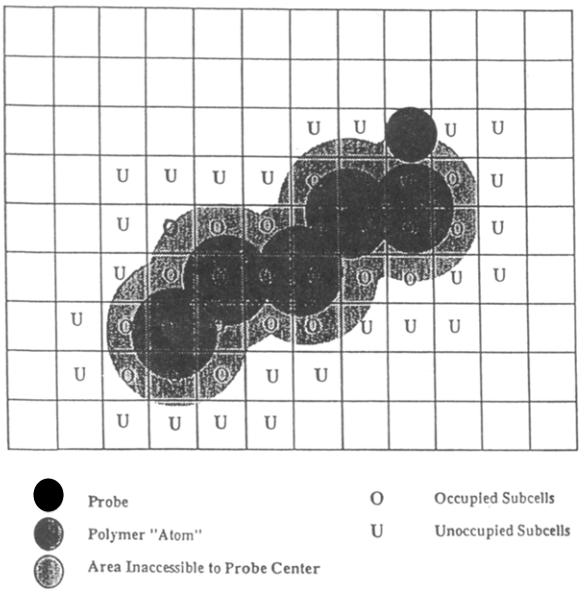

Figure 1. Schematic of the method used to delineate occupied and unoccupied subcells in the generation of free volume.

3. Results and Discussion

3.1. Free Volume Dependence on Probe Size. We examine the effect of the probe size upon the available free volume. In Figure 2 is shown the fraction of volume accessible to probes of different sizes in a *mixed*-PBD structure. For a point probe the free volume fraction is roughly 30.6% (nearly the same for all other PBDs). As the probe size increases, the available free volume decreases rapidly and approaches zero near a probe of radius 2 Å.

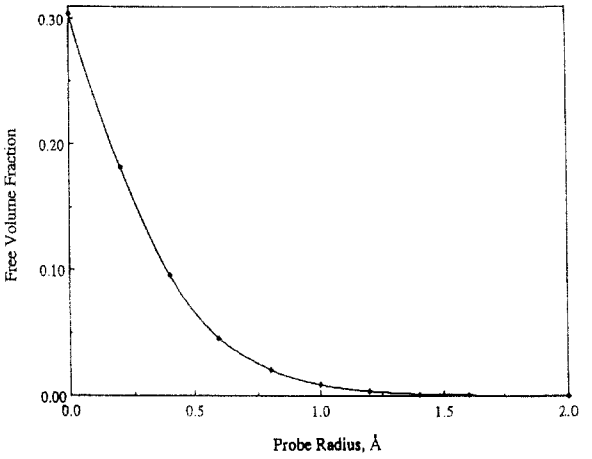

Figure 2. Free volume available to probes as a function of the probe size for *mixed*-PBD.

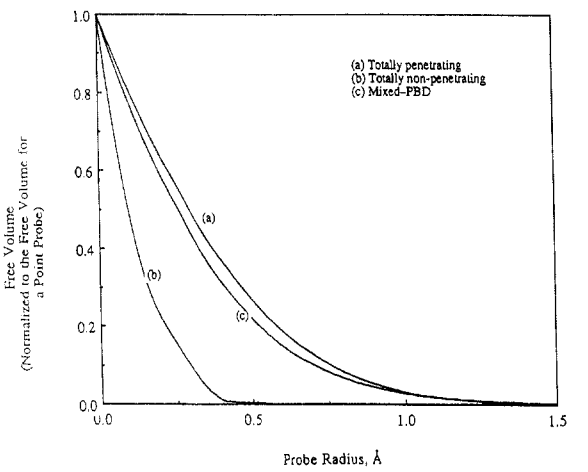

Figure 3. Free volume in *mixed*-PBD structure compared with the concentric shell theory of Rikvold and Stell[20] as a function of probe size. The spheres in the concentric shell model are assumed to have radii of 1.547 Å and 30.6% volume accessible to point probes. (a) Totally penetrating spheres, (b) totally nonpenetrating spheres, and (c) *mixed*-PBD amorphous cell.

The shape of the free volume curve is similar to that obtained by Shah et al.[15] and by Arizzi et al.[17] The free volume estimation visualized the carbon and hydrogen atoms as hard spheres. The shape of these curves should therefore be representative of the manner in which the hard spheres (carbon and hydrogen atoms) pack together.

Rikvold and Stell[20] have addressed the packing of hard spheres in a difference context. The concentric shell model of Rikvold and Stell relates the volume accessible to a probe of a finite radius to that available to a point probe (zero probe radius) in an assembly of hard spheres. The packed hard spheres can be in general partially penetrating (i.e., the distance of closest approach of the centers of two spheres can be less than the sphere diameter). While in the amorphous PBD cell one has hard spheres of three radii (sp^3 and sp^2 carbons and hydrogen atoms), a comparison of the Rikvold and Stell model with the predictions of the present work would shed light on the nature of the available free volume. For this purpose we assume that the polymer chains in the amorphous cell can be approximated as an assembly of hard spheres of radius 1.547 Å which has a 30.6% free volume accessible to a point probe (the same as that of a real PBD). The radius of 1.547 Å corresponds to 89% of the radius obtained by averaging over the sp^3 and sp^2 carbon atoms (40% of the spheres with 1.95-Å radius) and the hydrogen atoms (60% of the spheres with 1.598-Å radius). The two limits of totally penetrating spheres and nonpenetrating spheres are explored (corresponding respectively to eqs 6.5 and 6.6 in ref[20]). In Figure 3 are depicted the ratios of the free volume accessed by a finite size probe to that accessed by a point probe. It is immediately obvious that the behavior exhibited by the atomistic model can be mimicked quite well by an assembly of hard spheres. While the free volume in the assembly of nonpenetrating spheres drops much faster than that in an actual amorphous cell, the totally penetrating model predicts a slower drop off in free volume with increasing probe size. The free volume encountered in the amorphous cell could be represented as characteristic of an assembly of partially penetrating spheres. This results from the fact that the interatomic bonded distances are less than 89% of the sum of the van der Waals radii of the bonded atoms—the chemical bond thus forces the atoms to penetrate each other beyond 89% of their van der Waals radii. Thus in the amorphous cell the representation of carbon and hydrogen atoms is at least partially penetrating. The connectivity of the hard spheres seems to play a marginal role in that the total available free volume can be well represented by a disordered assembly of partially penetrating spheres without invoking bonding between the spheres, at least in this case where the chains are linear. Thus the nature of the free volume variation with the probe size is representative, to a first approximation, of an assembly of partially penetrating hard spheres.

Table I

structure	fraction	number-average size (Å^3)	volume-average size (Å^3)
cis	0.0095	1.09	16.11
trans	0.0078	0.85	9.32
vinyl	0.0131	1.60	32.60
mixed	0.0085	1.00	8.14

3.2. Free Volume Distributions. While the free volume decreases in quantity as the probe size increases, there is a qualitative change in structure of the free volume as well. This change would have direct implication on the penetrant diffusion. For a point probe the whole free volume is interconnected space. An infinite size void can still be found for a probe of radius 0.5 Å. As we increase the probe size, a percolation threshold is reached where the free volume breaks up into discrete, finite-sized, voids. For a probe radius of 1 Å the free volume is broken up into discrete voids (the threshold radius is between 0.5 and 1 Å). For a probe of radius 2 Å only one packet can be seen in the cell; the packets are smaller and, since they are fewer, are separated by large distances. Some part of penetrant dynamics involves periods of caging within voids and jumps between voids when, in the course of molecular dynamics, voids change shape and break up or combine.[21] The size of the voids must play an important role in this process since larger voids would facilitate the jump events compared to smaller voids. Thus the variation of the nature of the free volume with changing probe size provides an insight into the diffusion of the probes inside the amorphous polymer.

We further examine the free volume distribution probed by a hard sphere of radius 1 Å. (The radius of the orthopositronium, used frequently to probe the free volume, is 1.06 Å.[22]) Table I lists the total free volume fractions for the *cis*-, *trans*-, *vinyl*-, and *mixed*-PBDs. Also listed are the number-averaged and volume-averaged void sizes. While the free volume fractions of *cis*-, *trans*-, and *mixed*-PBDs are in the same range, the total free volume fraction in *vinyl*-PBD is significantly higher. Also while the number-average packet size is around 1 Å^3 for *cis*-,

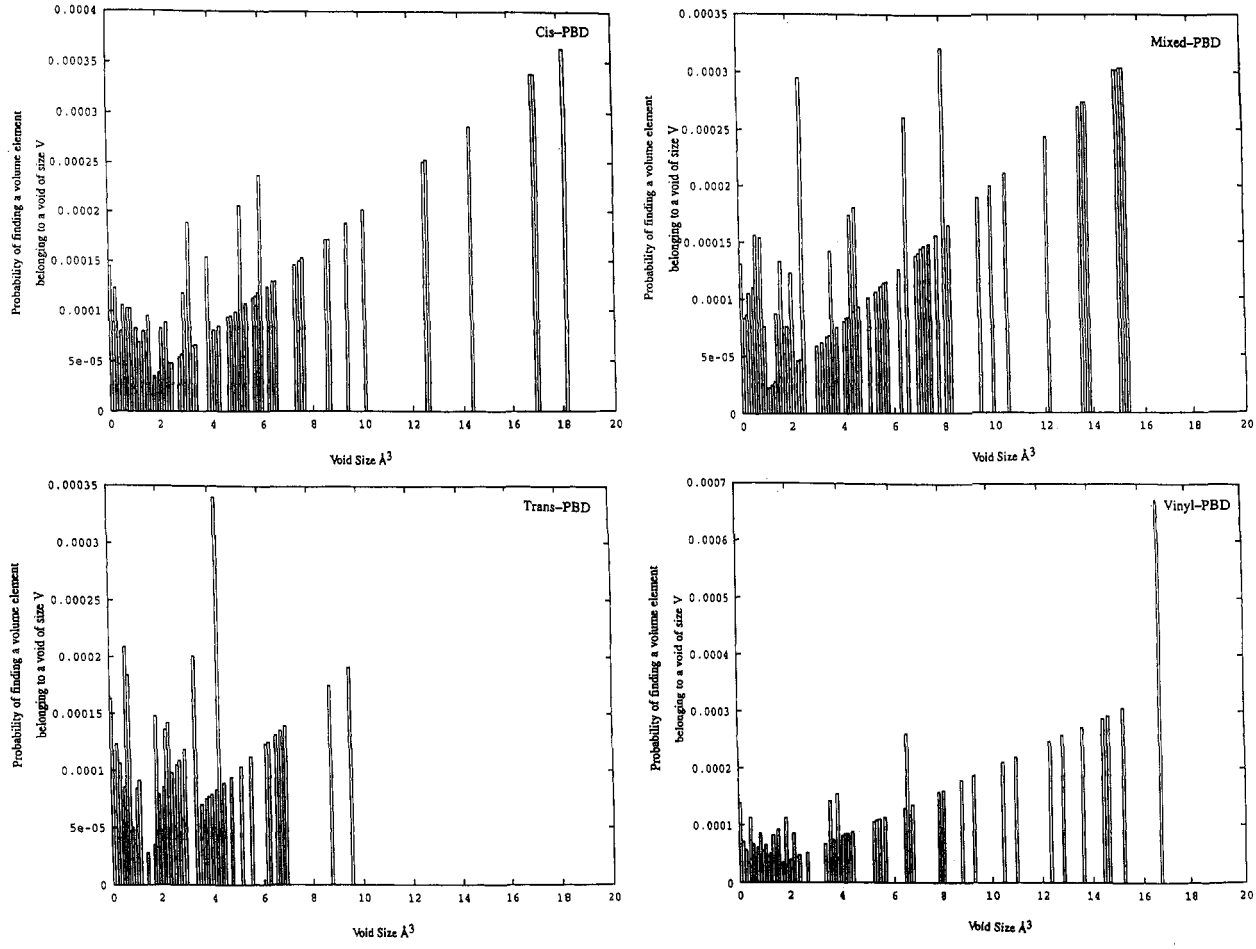

Figure 4. Free volume distributions (probe radius 1 Å) averaged over five amorphous cells for the case of (a) *cis*-PBD, (b) *mixed*-PBD, (c) *trans*-PBD, and (d) *vinyl*-PBD.

trans-, and *mixed*-PBDs, it is around 1.6 Å^3 for *vinyl*-PBD. The volume-averaged packet sizes are much higher, in the range 8–33 Å^3. This means that while there are numerous voids distributed throughout the polymer, most of the volume is contained by the fewer large packets. Another noteworthy aspect is the variation of the volume-average void size. While the *trans*- and *mixed*-PBD structures is is around 8–9 Å^3 and for *cis*-PBD around 16 Å^3, *vinyl*-PBD shows a very large void size of 33 Å^3.

Panels a–d of Figure 4 show the free volume distributions for various microstructures. To generate these figures free volume packets within size ranges of 0.1 Å^3 were grouped together. For example, free volume belonging to free volume packets between 0.1 and 0.2 Å^3 was assigned to a void size of 0.15 Å^3 and so on. The plots are in the form of the probability, $f_V(V)$, of a volume element belonging to a void of size V against the void size. The areas contained in the rectangles are thus the total free volume fractions, f (i.e., the probability that a given volume element belongs to *any* void).

$$f = \int_0^\infty dV\, f_V(V) \qquad (2)$$

The number of voids is limited to approximately 500 per microstructure, and therefore in any slice of 0.1 the number of voids is very small. At large void sizes (>10 Å^3) only a single void is present in each slice. Thus at this level of detail the probability seems to increase almost linearly with a few spikes. Indeed the error associated with each spike is about the same as the value of the probability itself. However, one can note a larger concentration of voids in the size range of ~7 Å^3 and also around 15–20 Å^3. The smoothed distributions are plotted

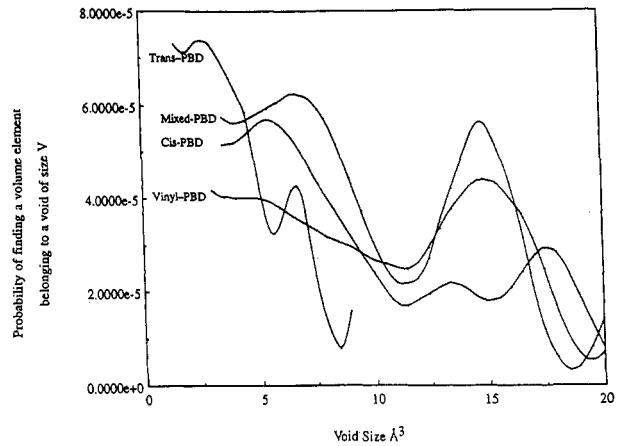

Figure 5. Smoothed free volume distributions corresponding to the distributions in Figure 4.

together in Figure 5. The smoothing was performed using a running average method with a three-point width, applied three times to the raw data. This procedure essentially takes the average of function values for an odd number of consecutive slices and assigns the average value to the middle slice. Two void size concentrations can in general be identified with each microstructure. One is the broad peak at a void size of ~7.5 Å^3 and another slightly above 15 Å^3. In the case of *trans*-PBD no voids above the size of 10 Å^3 are present, and so one can only identify the peak at 7.5 Å^3. In fact one can identify a peak at smaller voids which is absent in other structures—thus, although the amount of free volume has not changed substantially, it has been shifted to smaller sizes in *trans*-PBD. The figures show void distributions only up to 20 Å^3 to emphasize the

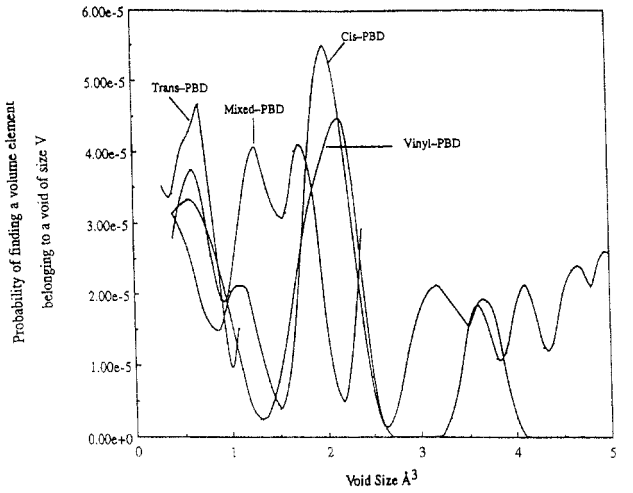

Figure 6. Smoothed free volume distributions corresponding to the distributions for a probe of radius 1.4 Å.

similarities and differences between microstructures of *cis*-, *mixed*-, *trans*-, and *vinyl*-PBDs. (*vinyl*-PBD shows one void each of size 42.45, 71.4, and 92.5 Å^3; hence the larger volume-averaged void size. *cis*-PBD shows one void each of size 30.2, 39.4, and 47.1 Å^3.)

One is also interested in the effect of the probe size upon the free volume distribution. For a probe size below the percolation threshold, most of the free volume is interconnected in an infinite void, while a probe of infinite size would yield a zero free volume. However, in between these two extremes the variation of the free volume distribution would be measurable. To explore the effect of probe size on the free volume distribution a probe of radius 1.4 Å was also used (the size of a water molecule). The smoothed distributions (Figure 6) reveal concentration of void sizes around 2 and 4 Å^3. Apparently, increasing the probe size shifts the free volume distribution to smaller void sizes and decreases the range of void sizes. The net effect of the probe size increase seems to be a shift and compression of the free volume distribution. This is because fewer cubelets can be occupied by larger probes.

3.3. Shape Analysis. While the size distribution gives us an estimate of the void sizes, it says nothing about the shapes of these voids. The shape of the voids is subjected to a twofold analysis. We measure the "roughness" of the void by comparing its surface to volume ratio to that of an equivalent sphere. The symmetry of the voids is measured by the asphericity and acylindricity of the voids. We also generated random aggregates of cubes on a grid similar to that employed for estimating the free volume in amorphous cells. These were grown by adding cubes to a vacant face selected randomly on a growing aggregate. The shape analysis of these random aggregates helps to elucidate the void shapes and is a measure of the departure of the void shapes from a random configuration of cubes.

3.3.1. Shape Factor Analysis. The shapes of the voids are studied as a function of their sizes. We define a so-called shape factor, S_V, for the voids which quantifies the departure of their shape from sphericity. With a given void one can associate a volume occupied by it, V, and the area of the surface enclosing that volume, S. One can then define the diameter of a sphere that would enclose the void, V, as

$$D_V = (6V/\pi)^{1/3} \tag{3a}$$

One can also define the diameter of a sphere that would be enclosed by a surface of area S as

$$D_S = (S/\pi)^{1/2} \tag{3b}$$

The shape factor S_V is then defined as the ratio

$$S_V = D_V/D_S \tag{4}$$

For a sphere the shape factor is unity and for any other shape it would be less than unity. For a cube the shape factor is 0.89. In Figure 7 shown is a scatter plot of shape factor versus the void size for all the microstructures. We expect that as the packet size increases, the shape gets increasingly distorted and the packets become more floppy. Indeed, one can observe the decrease in the shape factor with increasing void size, indicating increasing departure from sphericity. For the smallest voids the limiting value

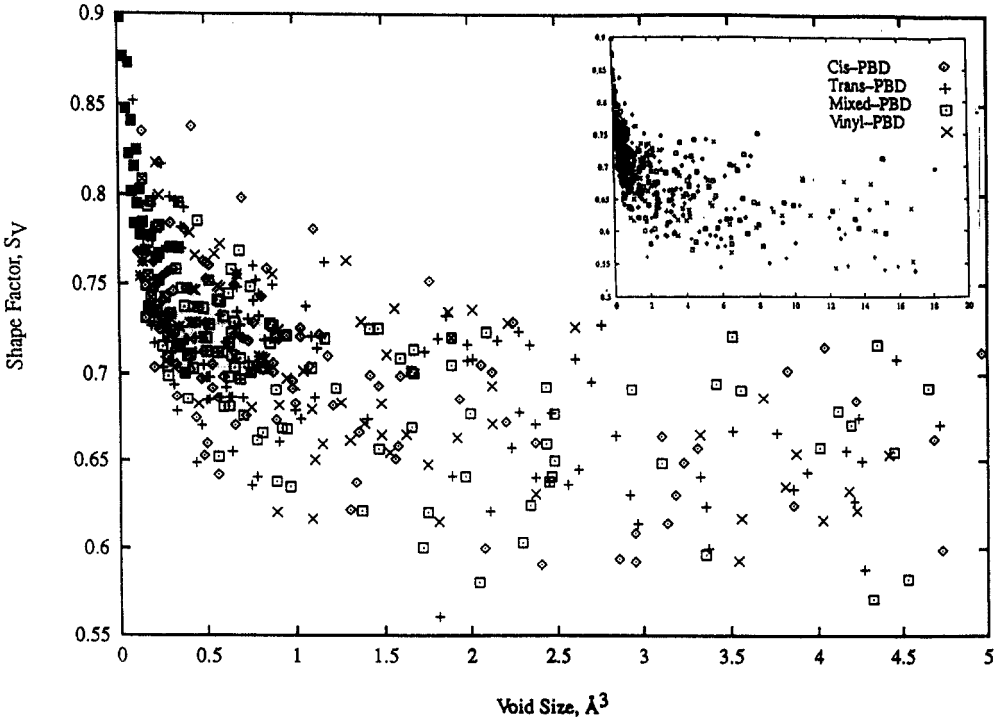

Figure 7. Shape factors of the voids as a function of the void size for all four PBDs (probe radius 1 Å). Inset shows shape factors for a larger range of void sizes (0–20 Å^3).

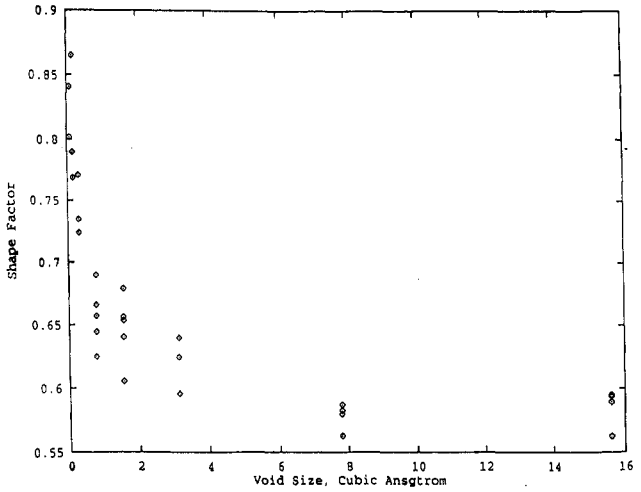

Figure 8. Shape factors for randomly grown aggregates of different sizes.

of the shape factor is 0.89 instead of unity. This limit results from the fact that the voids, in the current picture, are aggregates of cubic subcells, and thus the smallest void is just a cube with a shape factor of 0.89. Another prominent feature is that the average shape factor seems to decrease rapidly and reaches its asymptotic value at ~0.67 (the data seem to lie in a band of constant width between 0.57 and 0.75) at about a void size of 5 Å^2. Surprisingly, larger packets show no further distortion in shape. Given the scatter in the data, differences in the four microstructures are not distinguishable.

We now turn to a similar analysis on random aggregates of cubes. Aggregates of different sizes were grown randomly and for each size five aggregates were grown. The shape factors for these aggregates are shown in Figure 8. For aggregates up to 3 cubes (0.0469 Å^3) there is no scatter in the data since the shape factor is unchanging in any configuration of these cubes. As the aggregate size increases, the data show increasing scatter. However, as one approaches large aggregates of say 500 cubes (8 Å^3), the scatter decreases and the shape factor seems to tend to a limiting value in the range 0.56–0.59. The decay of the shape factor for random aggregates is also over the range of 0–5 Å^3. These numbers are very similar to those observed for the free volume voids. The range of 0.56–0.59 is the lower limit of the band of scattered shape factors for the voids. For the large void range the scatter is toward larger shape factors. The voids in the polymer structures are thus "smoother" compared to randomly generated shapes. Randomly grown clusters have lower shape factors due to larger corrugation of the surface compared to the actual voids. This is probably because the surfaces bounding the actual voids are formed by the neighboring carbon and hydrogen atoms, which have "smoother" spherical surfaces.

3.3.2. Symmetry Analysis. The shape factor alone does not completely define the shape of the voids. One is also interested in the shapes of these voids as compared to spheres and cylinders. The shapes of the polymer chains have been subjected to analyses which required measuring the radii of gyration of the chains along the principal axes

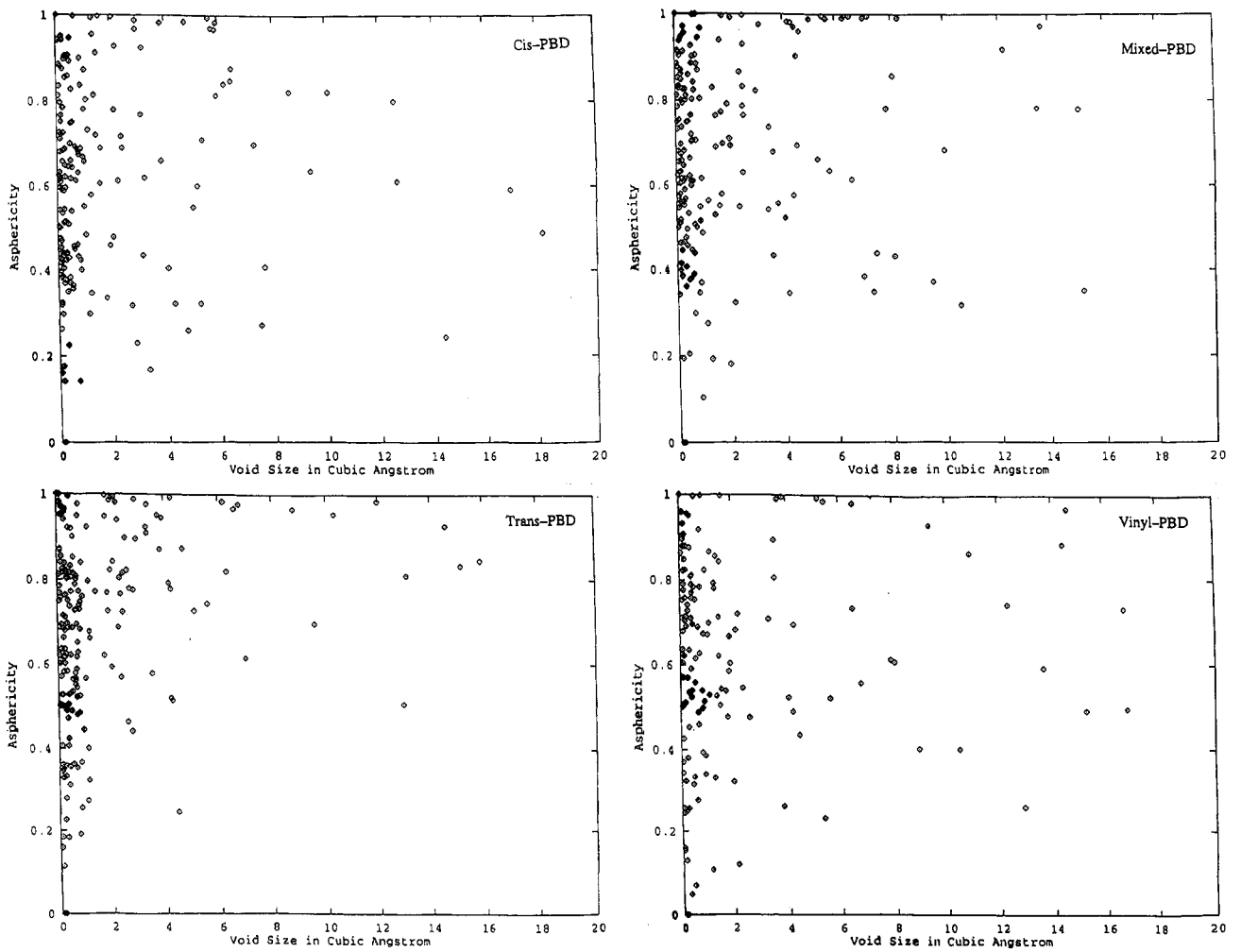

Figure 9. Asphericity of the voids (probe radius 1 Å) as a function of the void sizes for (a) *cis*-PBD, (b) *mixed*-PBD, (c) *trans*-PBD, and (d) *vinyl*-PBD.

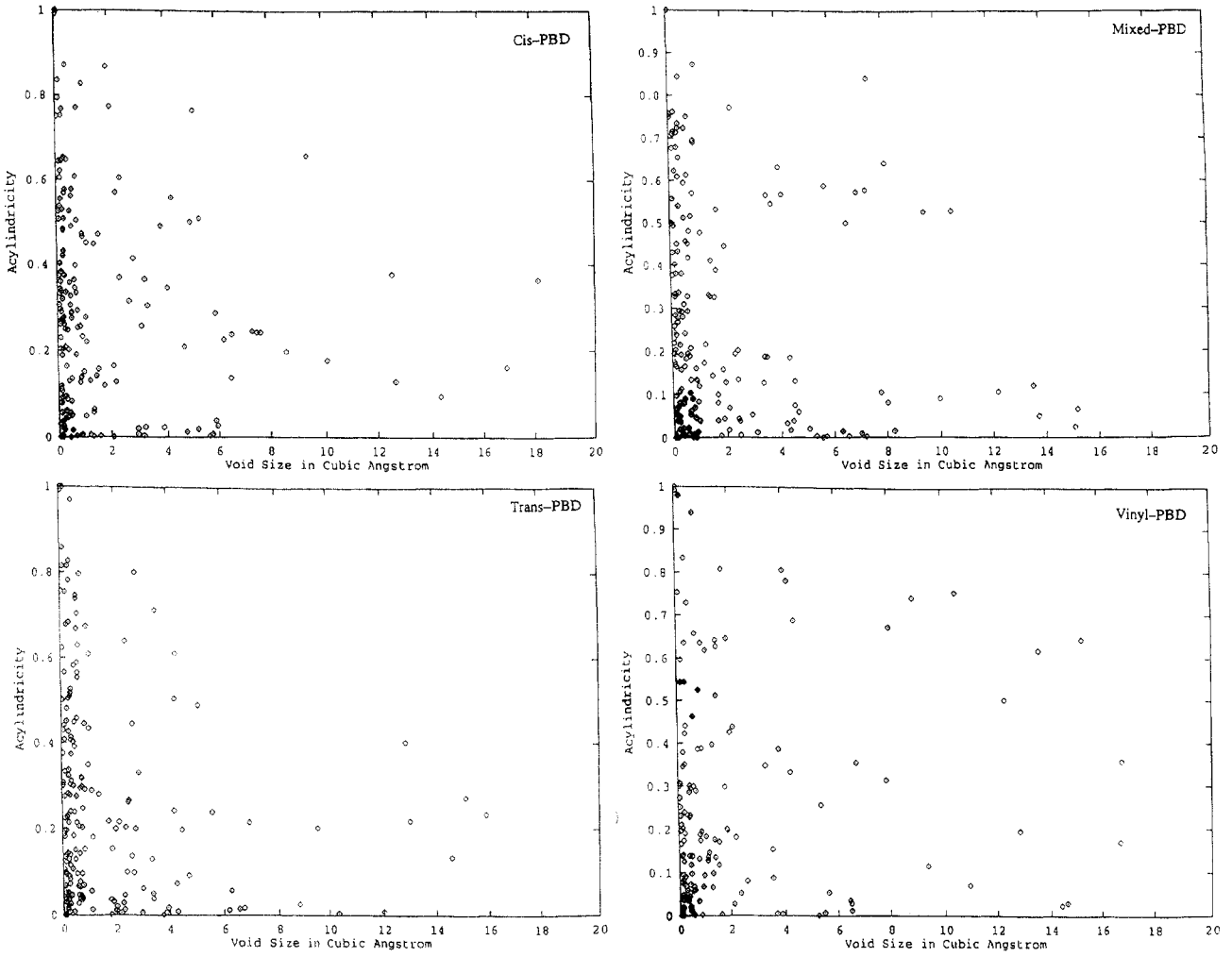

Figure 10. Acylindricity of the voids (probe radius 1 Å) as a function of the void sizes for (a) *cis*-PBD, (b) *mixed*-PBD, (c) *trans*-PBD, and (d) *vinyl*-PBD.

of inertia of the chains.[23-28] The same concepts can be applied to measuring the shapes of the voids as well. The radius of gyration tensor was computed for all voids and was transformed to the principal axis system (or diagonalized). For computing the elements of the tensor the center points of the cubelets were chosen. The eigenvalues of the radius of gyration tensor in descending order are $X \geq Y \geq Z$. We then scaled the eigenvalues by X to get a ratio of the radii of gyration, this procedure eliminating the "mass" dependence on subsequent analysis and focusing solely on the shapes. We now define two parameters as follows. The asphericity, σ, of the voids is defined as [28]

$$\sigma = 1 - {}^1/_2(\psi^2 + \zeta^2) \tag{5}$$

where $\psi = Y/X$ and $\zeta = Z/X$. We also define acylindricity, χ, of the voids as follows:[28]

$$\chi = \psi^2 - \zeta^2 \tag{6}$$

A void consisting of only one cube had $\sigma = 0$ and $\chi = 0$. A void consisting of two cubes had $\sigma = 1$ and $\chi = 0$. Large values of asphericity point to larger departure from spherical symmetry and to elongated voids, while a vanishing asphericity points to perfectly spherical shapes. Similarly, large acylindricity points to stubby voids, while low acylindricity is characteristic of elongated shapes.

In Figure 9 the asphericity of the voids is shown as a function of the void size for different microstructures. There is scatter at the lower void sizes. This is due to the strong fluctuations in shape. For example, while a void comprising one subcell is "spherical", that comprising two subcells is "cylindrical". The smaller voids can change shape drastically by little rearrangement; thus the strong fluctuations. In general, with increasing void size, the voids seem to become more cylindrical and less spherical. Interesting intermicrostructure differences appear at higher void volumes. *trans*-PBD (Figures 9c and 10c) and *mixed*-PBD (Figures 9b and 10b) show a larger population of cylindrical voids at large void sizes (>10 Å^3). *vinyl*-PBD, on the other hand, shows few cylindrical voids above 10 Å^3. *cis*-PBD has no cylindrical voids above 6 Å^3. Thus while the surfaces of the voids are almost equally corrugated or rough for all four microstructures, there is significant difference in the void shapes.

Figures 11 and 12 depict the asphericity and acylindricity, respectively, of aggregates grown randomly. There is large scatter for small aggregates, while large aggregates depart from spherical symmetry and become more cylindrical. However, one does not notice extremely long cylindrical random aggregates (like those in *trans*- and *mixed*-PBDs). This is because random aggregates are grown by adding cubes randomly and thus do not have a propensity to line up in long assemblies. On the other hand, in an amorphous cell the polymer chain connectivity can line up the voids into elongated shapes. Coupled with the symmetry analysis, one can infer that voids in polymer structures tend to be more cylindrical and have smoother surfaces compared to randomly grown shapes.

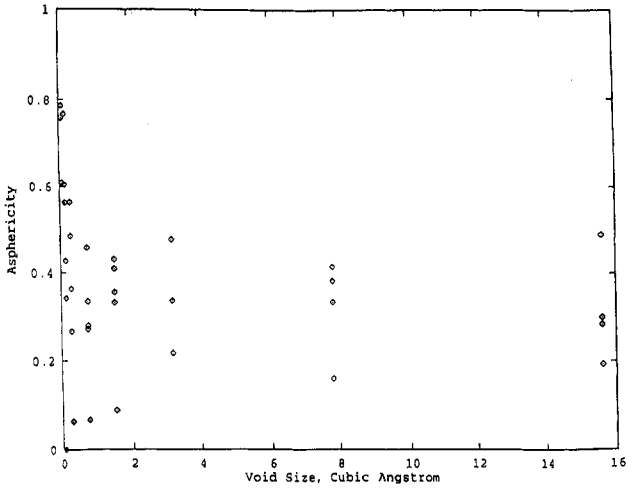

Figure 11. Asphericity of randomly grown aggregates of different sizes.

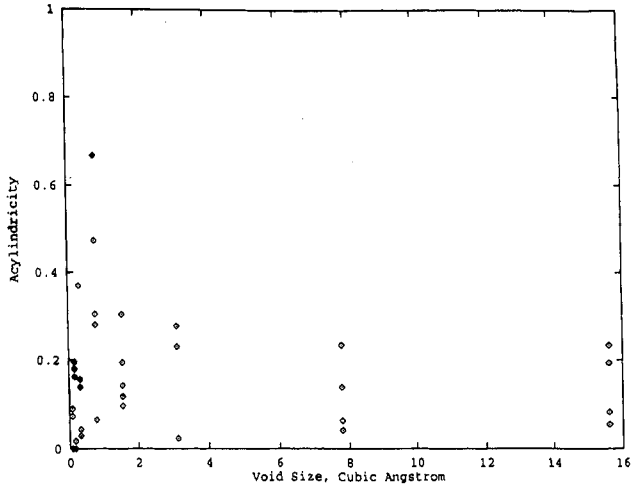

Figure 12. Acylindricity of randomly grown aggregates of different sizes.

4. Conclusions

Atomistically realistic models for amorphous poly(butadienes) have been generated and probed for free volume using hard spherical probes. Four microstructures, *cis*-PBD, *mixed*-PBD, *trans*-PBD, and *vinyl*-PBD, have been thus analyzed. The analysis reveals that the free volume available to hard probes is characteristic of volume available in disordered packings of partially penetrating spheres. The free volume distributions for all four microstructures (probed by a 1-Å-radius probe) in general show broad peaks around void sizes of 7.5 Å^3. All but *trans*-PBD also show a peak near 15 Å^3. The number- and volume-averaged sizes show variation however. The shapes of these voids have been subjected to further analyses. The shape factor decays rapidly from 0.89 to its limiting value of ~0.67 for all four microstructures over a void size range of ~5 Å^3. The analysis focusing on the asphericity and the acylindricity of the voids, however, reveals that pure *cis*-PBD and *vinyl*-PBD have few large elongated (cylindrical) voids compared to *trans*-PBD and *mixed*-PBD. Shapes generated by random aggregation of cubes form one limit of the void shapes in the PBDs.

Acknowledgment. This work was supported by grants from the Edison Polymer Innovation Corp. (EPIC) and by ARO 03-91-G-0047.

References and Notes

(1) Li, Y.; Mattice, W. L. *Macromolecules* **1992**, *25*, 4942.
(2) Kim, E. G.; Misra, S.; Mattice, W. L. *Macromolecules* **1993**, *26*, 3424.
(3) Nakanishi, H.; Jean, Y. C. *Macromolecules* **1991**, *24*, 6618.
(4) Meyer, E. F.; Jamieson, A. M.; Simha, R.; Palmen, J. H. M.; Booij, H. C.; Maurer, F. H. J. *Polymer* **1990**, *31*, 243.
(5) Shmorhun, M.; Jamieson, A. M.; Simha, R. *Polymer* **1990**, *31*, 812.
(6) English, A. D.; Zoller, P. *Macromolecules* **1986**, *19*, 2649.
(7) Sung, C. S. P.; Gould, I. R.; Turro, N. J. *Macromolecules* **1984**, *17*, 1447.
(8) Yu, W.-C.; Sung, C. S. P.; Robertson, R. E. *Macromolecules* **1988**, *21*, 355.
(9) Yu, W.-C.; Sung, C. S. P. *Macromolecules* **1988**, *21*, 365.
(10) Lomellini, P. *Polymer* **1992**, *33*, 4983.
(11) Cohen, M. H.; Turnbull, D. *J. Chem. Phys.* **1959**, *31*, 1164.
(12) Turnbull, D.; Cohen, M. H. *J. Chem. Phys.* **1961**, *34*, 120.
(13) Simha, R.; Somcynsky, T. *Macromolecules* **1969**, *2*, 342.
(14) Somcynsky, T.; Simha, R. *J. Appl. Phys.* **1971**, *42*, 4545.
(15) Shah, V. M.; Stern, S. A.; Ludovice, P. J. *Macromolecules* **1989**, *12*, 4660.
(16) Theodorou, D. N.; Suter, U. W. *Macromolecules* **1985**, *18*, 1467.
(17) Arizzi, S.; Mott, P. H.; Suter, U. W. *J. Polym. Sci., Polym. Phys. Ed.* **1992**, *30*, 415.
(18) Rigby, D.; Roe, R. J. *Macromolecules* **1990**, *23*, 5312.
(19) POLYGRAF v2.2, Molecular Simulations Inc.
(20) Rikvold, P. A.; Stell, G. *J. Colloid Interface Sci.* **1985**, *108*, 158.
(21) Sok, R. M.; Berendsen, H. J. C.; van Gunsteren, W. F. *J. Chem. Phys.* **1992**, *96*, 4699.
(22) Ache, H. J., in *Positronium and Muonium Chemistry*; Ache, H. J., Ed.; Advances in Chemistry Series 175; American Chemical Society: Washington, DC, 1979; p 2.
(23) Solc, K.; Stockmayer, W. H. *J. Chem. Phys.* **1971**, *54*, 2756.
(24) Solc, K. *J. Chem. Phys.* **1971**, *55*, 335.
(25) Yoon, D. Y.; Flory, P. J. *J. Chem. Phys.* **1974**, *61*, 5366.
(26) Mattice, W. L. *J. Am. Chem. Soc.* **1979**, *101*, 732.
(27) Mattice, W. L. *J. Am. Chem. Soc.* **1979**, *101*, 7651.
(28) Theodorou, D. N.; Suter, U. W. *Macromolecules* **1985**, *18*, 1206.